# A Hand-Held, Intra-Operative Positron Imaging Probe for Surgical Applications

Hamid Sabet, *Member, IEEE*, Brendan C. Stack Jr., and Vivek V. Nagarkar, *Member, IEEE*

***Abstract*—We have developed a prototype intra-operative $\beta^+$ imaging probe to help tumor removal and malignant tissue resection. The probe can be used during surgery to provide clear delineation of malignant tissues. Our probe consists of a hybrid scintillator coupled to a silicon photomultiplier (SiPM) array with associated front-end electronics encapsulated in an ergonomic aluminum housing. Pulse shape discrimination electronics has been implemented and integrated into the downstream data acquisition system. The field of view of the probe is $10 \times 10$ mm$^2$ realized by a 0.4 mm thick CsI:Tl scintillator coupled to a 1 mm thick LYSO. While CsI:Tl layer acts as $\beta^+$ sensitive detector, LYSO detects gamma radiation where the gamma response can be subtracted from the total signal to improve SNR and contrast. The thickness of the LYSO scintillator is optimized such that it acts as light diffuser to spread the scintillation light generated in CsI:Tl over multiple SiPM pixels for accurate estimation of the $\beta^+$ interaction location. The probe shows $<$ 1 mm FWHM spatial resolution in the presence of large background radiation. The probe was used to study rabbits with tongue tumors. The experimental results show that the probe can successfully locate the tongue tumors in its active imaging area.**

***Index Terms*—Handheld, hybrid scintillator, imaging positron probe, intra-operative, pulse shape discrimination, SiPM.**

## I. Introduction

STAGING and restaging of cancer has significant importance in planning patient's recovery and prognosis. Tumor removal is a complicated procedure in that normally the bulk of the tumor, and not its margin, is identified and removed. This procedure is typically accompanied by multiple biopsies during the surgery to analyze the tumor margins and confirm whether there is a need for more tissue resection. This time-consuming procedure normally leads to higher patient and hospital costs. Since the patient can be anesthetized for a limited time, the number of biopsy iterations is limited. Therefore there is always a chance that the tumor is not completely removed during the first surgery which translates to increased hospital utilization and cost, and longer patient recovery.

Manuscript received October 17, 2014; revised January 22, 2015; accepted June 11, 2015. Date of publication August 25, 2015; date of current version October 09, 2015. This work was supported in part by the U.S. National Institute of Health under Grant 1R43CA168100-01A1.

H. Sabet was with RMD Inc., Watertown, MA 02472 USA. He is now with Massachusetts General Hospital, Harvard Medical School, Charlestown, MA 02129 USA (e-mail: HSabet@MGH.Harvard.edu).

B. C. Stack Jr. is with Medical Sciences, Univeristy of Arkansas, Little Rock, AR 72205 USA.

V. V. Nagarkar is with RMD Inc., Watertown, MA 02472 USA.

Color versions of one or more of the figures in this paper are available online at http://ieeexplore.ieee.org.

Digital Object Identifier 10.1109/TNS.2015.2446434

Image-guided surgery has gained tremendous attention in recent years and spans over a range of technologies such as radiotracer- and optical based imaging modalities. Near infrared (NIR) fluorescence imaging falls into the latter category and is based on utilizing light photons at the 700-900 nm range that can penetrate a few millimeter in tissue with minimal absorption and scattering. While NIR is promising in certain surgical applications, much research has yet to be done in order to make that a viable technique that can be used for various clinical applications [1].

Radiotracer-guided intra-operative probes can potentially increase the specificity of tissue biopsies, enable minimal-access incisions, reduce patient hospital utilization, and contribute to improved patient recovery. The excision of all tumor tissue is important for the recovery, health and even survival of the patient [2].

Intraoperative probes have been used in the treatment of cutaneous melanoma, squamous cell carcinoma, breast carcinoma, thyroid tumors, and parathyroid adenoma. Various groups have designed imaging, and non-imaging probes using scintillation- or semiconductor-based detectors [3]–[20]. However, most of the available probes are non-imaging, and cannot clearly provide information about the boundaries of the surveyed malignant tissue. Furthermore, most of the probes available at the hospitals are only sensitive to gamma radiation and are used in conjunction with radiopharmaceuticals such as $^{99m}$Tc, $^{131}$I, $^{111}$In, or $^{125}$I. One major limitation of the gamma probes is that their ability to detect the radiolabeled residual tumor can be strongly hampered due to the gamma background contamination. Background contamination exists in healthy tissues surrounding the tumor or in organs with large radiotracer uptake such as heart, bladder, and brain. The spatial resolution of gamma probes deteriorates with increasing tissue-probe distance. The degradation of spatial resolution can be controlled using a collimator to limit the FOV, however leads to loss in sensitivity. Therefore the gamma probes are most commonly used to identify the sentinel lymph nodes where the radiotracer is intratumorally injected to the tumor site which limits the tracer spread. On the other hand many of the recently designed probes for tumor margin detection are sensitive to $\beta$ radiation and are capable of rejecting 511 keV gamma background [3], [5], [14], and [16].

RMD has previously designed an imaging $\beta$ probe with no gamma background rejection by coupling microcolumnar CsI:Tl scintillator to a CCD camera [21][22]. While the structured scintillator used in the design provides high spatial resolution, the CCD camera is bulky and requires dedicated

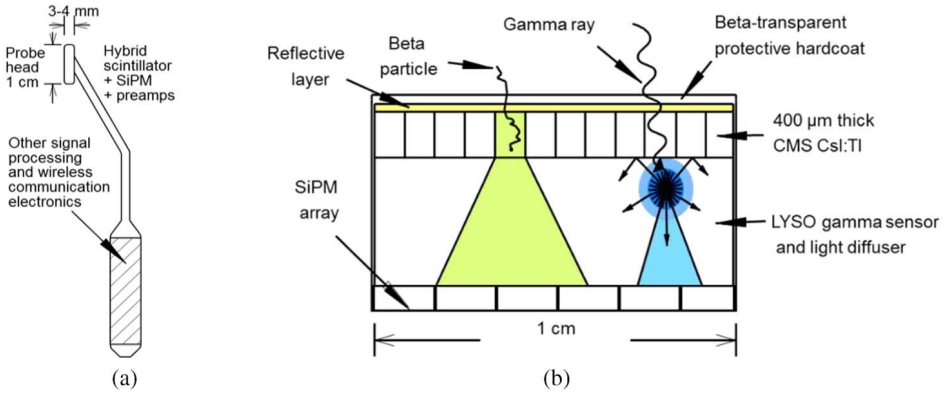


Fig. 1. (a) Conceptual design of the imaging probe head. (b) The ultimate probe design which realizes a wireless handheld unit.

cooling system which can limit the probe application. By the emergence of new photodetector technologies such as silicon photomultipliers (SiPMs), development of compact and cost-effective imaging probes is now practical. We adapted these new technologies to develop high performance detectors for intra-operative imaging $\beta$-sensitive probe called Imaging Beta probe (IPB). In the first version of the probe, we have utilized a SiPM array and CsI:Tl scintillator grown in the form of pixelated array to achieve position sensitivity [23]. In the current work, however, we present a novel beta probe that utilizes hybrid scintillator for improved SNR and image contrast by subtracting the gamma background from the $\beta$ response. This approach would be particularly effective when the probe is used near organs with high radiotracer uptakes, such as the bladder, heart, or brain, and can therefore generate large 511 keV background that easily prevails over the $\beta$ signal. The probe is designed to rapidly localize tumor and provide a near real-time and high resolution image of the surveyed areas by sensing $\beta$ radiation and rejecting the gamma background. With respect to other $\beta$ probes reported elsewhere, our design provides a more robust and less complicated platform in that we use finely pixelated and high light yield scintillator (CsI:Tl) directly coupled with SiPM array. This geometry yields larger light collection which provides a high sensitivity for detecting weak $\beta$ in presence of large background radiation.

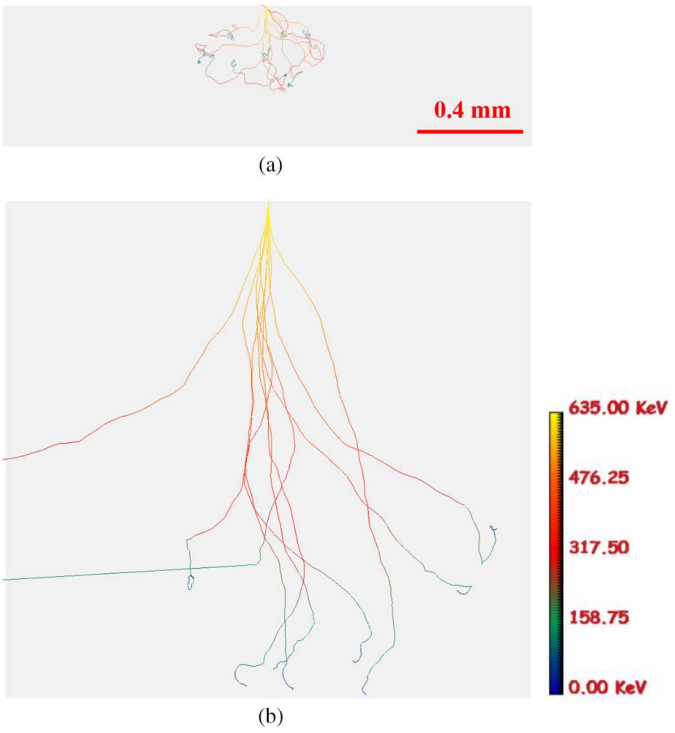


Fig. 2. Range of F-18 positrons in CsI:Tl (a) and water (b). For clarity, we only show trajectories of 10 electrons at 635 keV. We utilized CASINO simulation software available at [25].

## II. Probe Design

The conceptual design of the intra-operative probe is shown in Fig. 1(a) where we envisage a compact detector together with its associated front-end electronics placed inside an ergonomic housing. The detector signals will be first processed locally and then will be sent to downstream electronics using a wireless transmitter.

We built the first prototype of the probe where the probe is connected to downstream electronics using a Flexible Flat Cable (FFC). In this design, the probe head is comprised of a hybrid scintillator in that a 0.4 mm thick pixelated CsI:Tl is coupled to a 1.0 mm thick monolithic LYSO:Ce scintillator (see Fig. 1(b)). CsI:Tl primarily senses the $\beta$ particles originating from the $^{18}$FDG radiotracer. This thickness is sufficient to stop more than 95% of the positrons in $^{18}$FDG. Positrons in F-18 can travel up to 2.4 mm in water before completely absorbed [24]. Fig. 2 shows a comparison of positron range in CsI:Tl and water (tissue) using CASINO simulation package [25]. The results show a maximum projected range of 0.47 mm in CsI:Tl which is in good agreement with the literature [26]. It is apparent that using CsI:Tl as the beta-sensor has clear advantage compared to other scintillators (e.g. plastic) reported elsewhere. A 0.4 mm thick CsI:Tl layer provides a high stopping power while enabling a compact probe head design. Furthermore, CsI:Tl has a high light yield (53 photons/keV) compared to that of the plastic scintillator ($\sim$ 10 photons/keV). The expected number of scintillation photons generated by incident positrons with maximum and average energies of 635 and 250 keV is $\sim$ 33000 and $\sim$ 13000. The high light output of

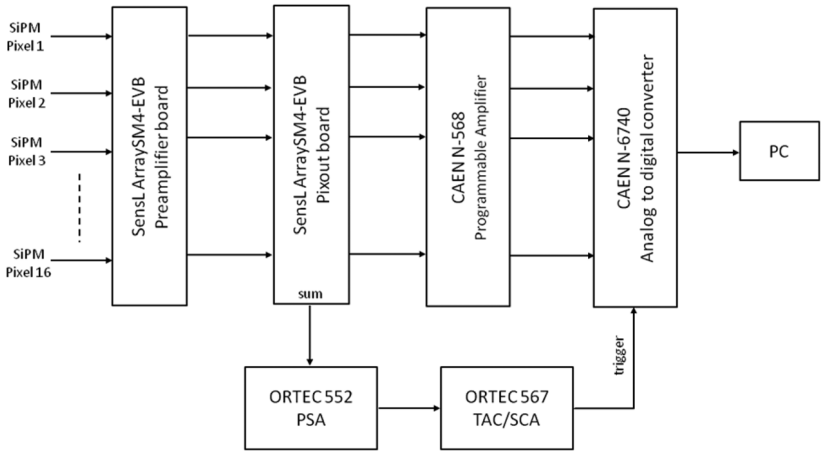


Fig. 3. Data acquisition setup for generating 2D position histogram, 1D line profiles and energy spectra. Note that pulse shape discrimination is implemented using ORTEC 552 PSA and 567 TAC/SCA units. This allows to trigger the ADC unit when the signal is originating from CsI:Tl scintillator.

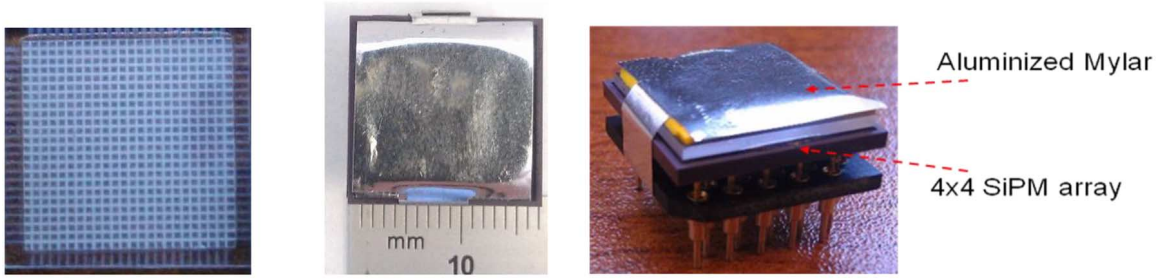


Fig. 4. (a) Photo of a fabricated hybrid scintillator. A 400 $\mu$m thick CsI:Tl is optically glued to 1 mm thick LYSO:Ce. This thickness is sufficient to stop $> 95\%$ of the positrons in $^{18}$FDG source. The CsI:Tl is laser pixelated into $0.5 \times 0.5$ mm$^2$ pixels. (b) top view of the packaged detector with a 12.5 $\mu$m thick aluminized mylar on top. (c) a photo of the packaged detector comprising the hybrid scintillator, coupled to SiPM array. Note that the detector sits on to an interface terminal socket.

CsI:Tl, together with its small thickness are in favor of light collection at the photodetector plane. Assuming that only one third of the scintillation photons reach the photodetector and considering a %15 quantum efficiency at 550 nm (peak emission wavelength of CsI:Tl), there will be $\sim$ 650 photons collected by the photodetectors for a positron with 250 keV energy.

In our design, LYSO:Ce detects the 511 keV gamma photons which can be used to correct the beta image for improved contrast and SNR. Owing to the large difference in decay time of CsI:Tl (1000 ns) and LYSO:Ce (40 ns), we applied pulse shape discrimination (PSD) to the SiPM signals to discriminate against background 511 keV gammas.

We used ArraySM-4, a SensL SiPM which has a $4 \times 4$ array of pixels each $3 \times 3$ mm$^2$ with 3.36 mm pixel pitch. The effective area of the array is $13 \times 13$ mm$^2$ with 54% fill factor. The surface of the SiPM array is protected by a 0.5 mm thick optical coating. We used ArraySM4-EVB-PreAmp, a 16 channel preamplifier board which is a compact and low profile base to accommodate the SiPM array with onboard amplifiers. This board delivers the SiPM signals to the downstream electronics through a 1-meter long FFC. At the beginning of the downstream electronics is ArraySM4-EVB-Pixout, SensL's breakout board that provides sum of all SiPM signals along with easy access to individual SiPM signals. The signals are then shaped and further amplified by a 16-channel spectroscopy amplifier. The output signals of this board are then fed to a multi-channel analog-to-digital converter (ADC). The sum of all signals in the breakout board is further processed by PSD circuit, and then is used to trigger the ADC unit. We incorporated PSD using modular Nuclear Instrumentation Module (NIM) bins. The schematic diagram of the data acquisition system is shown in Fig. 3. A simple Anger logic (centroid method) is applied to the 16 signals to estimate the position of $\beta$ interaction. In our design, $10 \times 10 \times 0.4$ mm$^3$ CsI:Tl slabs are optically glued to $12 \times 12 \times 1$ mm$^3$ LYSO crystal (see Fig. 4(a)). The CsI:Tl scintillator is then pixelated to $0.5 \times 0.5$ mm$^2$ pixels to limit the light spread using laser ablation technique [27][28]. The pixelation time was 17 minutes and 49 seconds which is very fast compared with other pixelation techniques for such fine pixel size. Noteworthy that the actual pixelation time was only 2 minutes and 49 seconds, and the remaining 15 minutes was rest-time for the optical glue. This time was necessary to avoid CsI:Tl slab delaminating from the LYSO substrate. A photo of the fabricated hybrid scintillator is shown in Fig. 4(a). The resultant inter-pixel gap is filled by MgO powder to enhance the light reflection from the pixel walls. A 12.5 $\mu$m thick aluminized Mylar was placed on the top surface of the hybrid scintillator to reflect the scintillation light back towards the SiPM array and thereby improve light collection. The

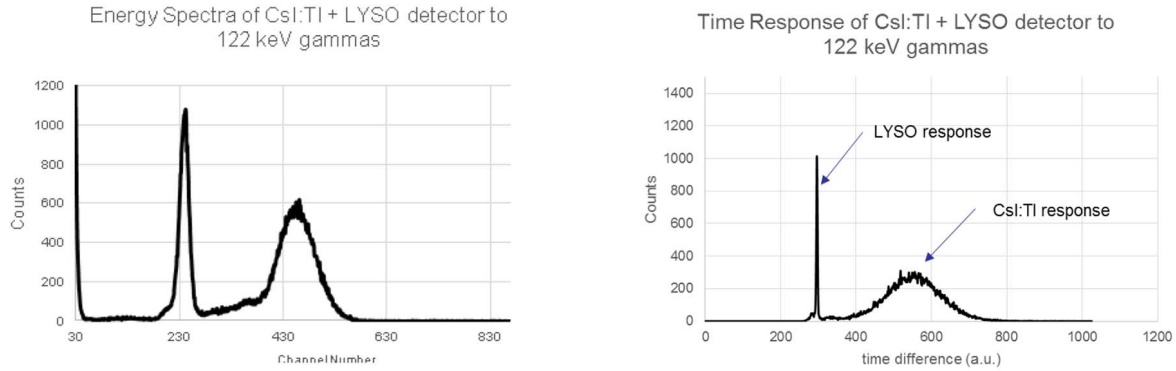


Fig. 5. Energy and time spectra of the hybrid scintillator exposed to 122 keV gammas. Due to the longer decay time of the CsI"Tl, one can reject the LYSO signal using PSD.

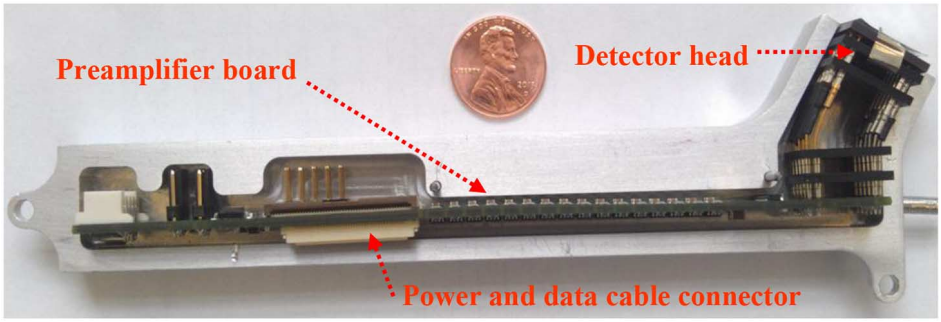


Fig. 6. Photo of the prototype probe consisting of detector head, PreAmp board, and aluminum housing.

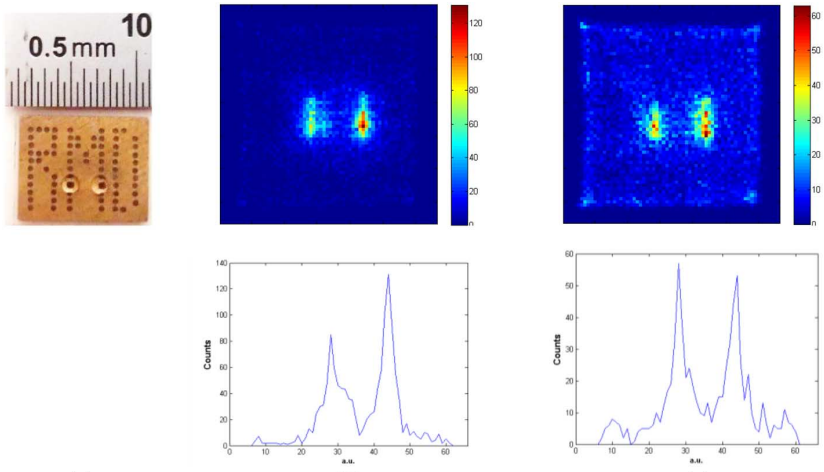


(a) (b) (c)

Fig. 7. (a) photo of a phantom with RMD letters with two drops of F-18. Images and their associated line profiles of the two drops are shown without and with gamma background in b and c, respectively. Note that the images are with PSD electronics applied. The gamma background was a 414 $\mu$Ci Ge-68 rod source placed at 3 cm from the probe head. The center-center distance of the holes is 2.3 mm. As depicted from a, each F-18 drop covers 2 holes and their associated images are elongated along the covered holes. In b, the calculated spatial resolution for the two peaks from left to right is 0.94 mm and 0.67 mm FWHM. This value is 0.73 mm and 0.8 mm FWHM for the line profile in c. Note that the two F-18 drops could not be identified if no PSD electronic was applied.

hybrid scintillator was optically coupled to the SiPM array using a Dow Corning Q2-3067 optical gel. Fig. 4(b) and (c) represent photos of the packaged sensor head.

After assembling the detector head we tuned the PSD electronics to effectively eliminate the signals originated in LYSO:Ce. No pulse height discrimination (PHD) was applied, and LYSO signal was filtered only by PSD electronics based on shorter decay time of LYSO compared with CsI:Tl (see Fig. 5).

Compact and ergonomic Aluminum housing was machined to accommodate the detector head and the preamplifier electronic board. The design of the housing is based on compactness, light weight, and angulation of the probe head for easier access to the intended locations. A photo of the prototype of the detector head and its housing is shown in Fig. 6. Note that the probe head is at 30° with respect to the probe body to improve access to the tumor locations.

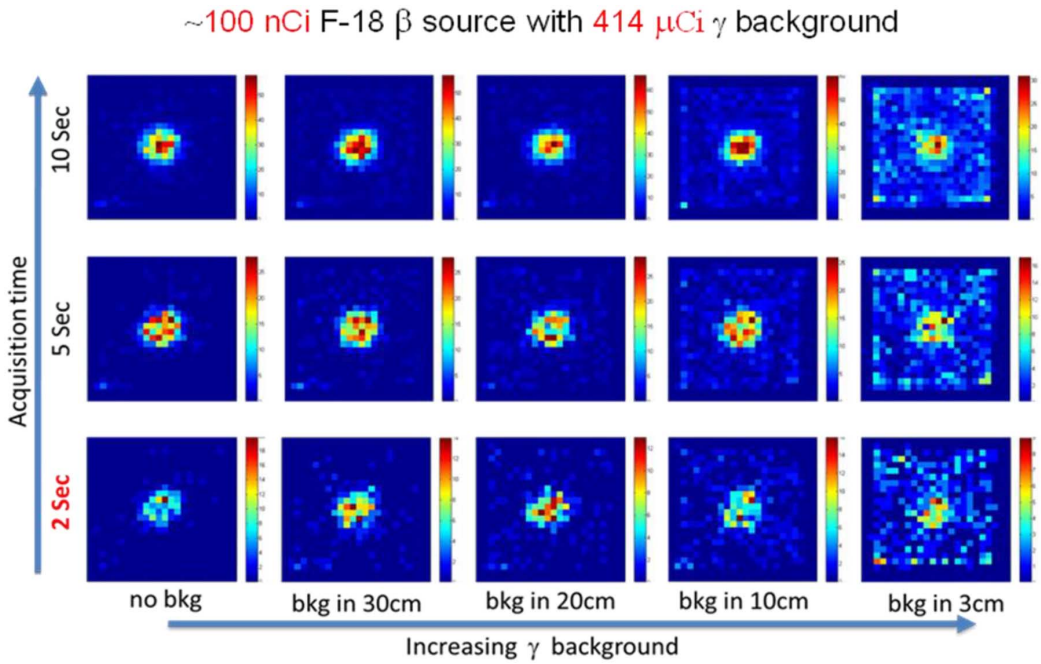


Fig. 8. Acquisition time versus increasing gamma background strength. No smoothing or baseline correction was applied to the results. The data show that the probe can comfortably detect beta signal with 10 second acquisition time at all background distance. However, SNR and the quality of the image reduce dramatically with short acquisition times (e.g. 2 seconds) and short background-detector distances.

## III. Probe Characterization

### A. Spatial Resolution

The probe was characterized using phantoms prior to animal imaging. Spatial resolution of the probe was tested using a 1 mm thick brass phantom with RMD letters. The letters comprise of through holes with 0.5 mm diameter and $\sim$ 1.1 mm center-to-center distance. The phantom was wrapped in a layer of Scotch tape to avoid contamination with radiotracer. Two F-18 drops (see Fig. 7(a)) with total activity of 1.8 $\mu$Ci were placed on the phantom. As seen in the picture, each F-18 drop covered multiple phantom holes. Note that the center-to-center distance between the phantom holes with F-18 drops is 2.3 mm. We used a 414 $\mu$Ci Ge-68 calibration rod source as gamma-ray background sitting at 3 cm distance from the probe head. This distance is selected to simulate an organ with high uptake in the proximity of tumor and not for generating flood image. The phantom with the two drops was placed directly on the probe head. Note that in this configuration, the F-18 positrons from the two drops can travel through the holes of the phantom and absorbed in the CsI:Tl scintillator. Data was acquired for the following scenarios: 1) no gamma background (i.e. Ge-68), and 2) with background and PSD applied. For each scenario, data was acquired for 10 seconds. The results are presented in Fig. 7(b)–7(c). The results demonstrate that the two F-18 drops are well separated in the image acquired in presence of background radiation. In the 1D line profiles, a spatial resolution of 0.8 mm FWHM is calculated. No data correction technique was used to generate the images.

### B. Acquisition Time

We evaluated the ability of the probe to generate an image as a function of acquisition time. We placed a single F-18 drop measured at 100nCi on Scotch tape positioned on to the probe head. The Ge-68 rod source was used to imitate $\gamma$ background. We acquired image of the F-18 drop with 10, 5, and 2 second acquisition time. For each acquisition time, we acquired data under five scenarios: no background, and background source sitting at 30, 20, 10 and 3 cm from the F-18 drop. The results (see Fig. 8) show that the shorter the acquisition time and/or the shorter the detector-background distance, the SNR and hence the image quality worsen.

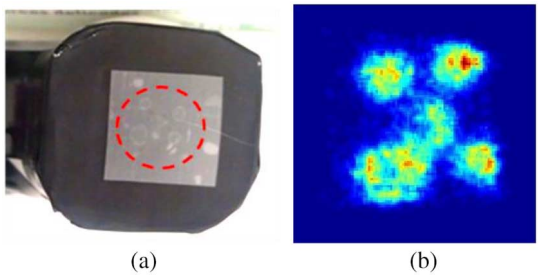


Fig. 9. (a) five F-18 drops, with total activity of $\sim$ 10 nCi placed on Scotch tape. (b) acquired image of the drops showing that the probe can detect weak beta signals.

### C. Sensitivity

We placed 5 F-18 drops on Scotch tape sitting on the probe head. The total activity was measured at $\sim$ 10 nCi. A separate Scotch tape containing a 400 nCi F-18 drop was kept at 3 cm distance from the probe head (see Fig. 9). A 30 second data acquisition shows that the probe can effectively pick up nano-Curie level of $\beta$ particles in presence of relatively large gamma background.

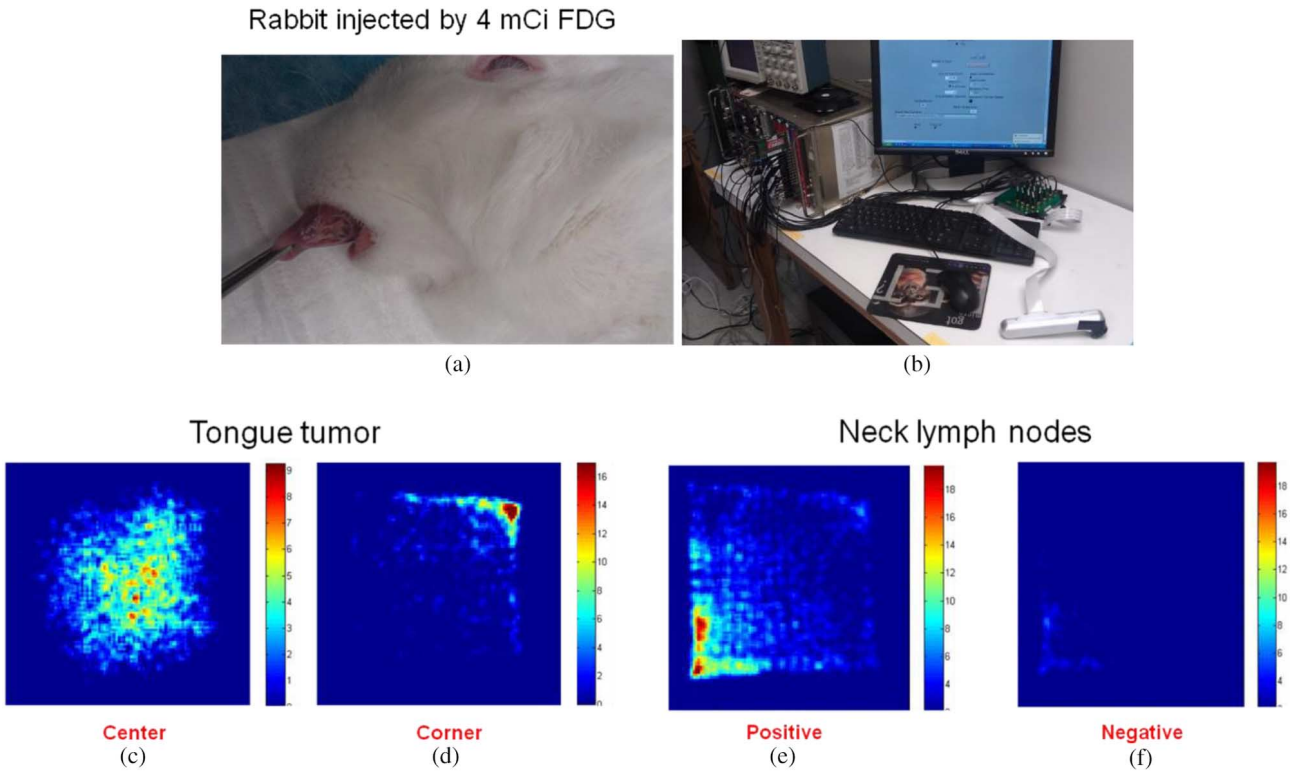


Fig. 10. (a) The rabbit with tongue tumor. Tumor cells were injected to the animal's tongue two weeks before the experiment. (b) photo of the probe with associated electronics and display. (c) and (d) show images of the tongue tumor and how the probe can be used to locate the tumor margin. (e) and (f) show images of the positive and negative lymph nodes in rabbit's neck. The results suggest that the probe can be used to check the status of the lymph nodes ex-vivo.

## IV. Animal Study

We performed animal imaging on rabbits with tongue tumors. The rabbit was injected by 15 million VX tumor cells two weeks before imaging/incision procedure. Tumor grew to $\sim$ 12 mm diameter in the two weeks period. This is a validated orthotopic model for head and neck tumors which is based on creating a model of a common cancer, with a normal primary tumor site that spreads pathophysiologically similar to human [29]. Our previous studies also suggest that cancer metastasize to lymph nodes in the rabbit's neck in about two weeks. On the day of procedure, the rabbit was intravenously injected by $\sim$ 4 mCi of $^{18}$FDG. Two hours post-injection, we performed a PET scan to image the tumor and to observe whether the neck lymph nodes are detected in the image.

During the animal study, we covered the probe by a thin latex cover used for ultra-sound imaging to avoid probe contamination from body fluids. The probe was used to acquire a series of images with user-selectable acquisition time. We placed the probe with respect to the tumor in center, and corner positions followed by a 10 seconds acquisition time. Fig. 10(c) and 10(d) show the results where the probe can clearly provide the location of the tumor and its margin. We also imaged the lymph nodes in the rabbit's neck. We removed the nodes, placed them in one corner of the probe, and acquired image for 30 seconds. The results (see Fig. 10(e) and 10(f)) show that the positive lymph node can be effectively distinguished ex-vivo from the negative node based on the number of counts. It should be noted that 10 second acquisition time for the lymph node resulted in a noisy image such that they could not provide meaningful information about the nodes.

## V. Discussion and Conclusion

In this work, we reported the first results of our recently developed intra-operative imaging probe dedicated to tumor removal. We showed the capability of the prototype probe to detect weak $\beta$ signals in presence of large gamma background. In the current design, we utilized general purpose NIM-bin modules for the downstream electronics; however we believe that by incorporating a dedicated and compact electronics that sits comfortably inside the probe housing can improve the overall performance. We also anticipate that by utilizing a SiPM device with improved QE and PDE, one would achieve an improved performance in all metrics. In the current design we did not incorporate any means to compensate for temperature fluctuations that can adversely affect the performance of the SiPM and thus the image quality. Moreover, new SiPM devices have thin ($<$ 0.1 mm) optical coating leading to smaller light spread in the coating layer. Thin coating layer also allows for using thicker LYSO:Ce crystal to improve detection sensitivity of gamma rays that can be used to enhanced correction for beta image. However using thick LYSO:Ce, due to the natural background radiation of Lu-176, may result in unwanted interaction in CsI:Tl layer which can degrade the probe's performance.

As described in the probe characterization section, we used Scotch tape in all measurements to separate the □ source and the probe head. The thickness of Scotch tape is similar to that of

the latex glove covering the probe during animal study to avoid contamination.

In the current probe prototype, we have not used any collimator or shielding; however, considering side and back shielding for the probe head with an optimized geometry can be important. The importance of these shielding is more pronounced for surveying an intended target in close proximity of organs with high radiotracer uptake. During the in-situ imaging of the tumor, the quality of the image was dependent on the direction of the probe head with respect to the rabbit body which suggest that a proper side and back shielding is a must for future experiments. In Fig. 10 we demonstrate the ability of the probe to provide an image of the tumor with respect to its location from the center of FOV. However similar to other imaging modalities, we conclude that it is best to position the tumor in the center of FOV to avoid image truncation at the detector edge (see Fig. 10(d)).

The images of the nodes provided meaningful information only in ex-vivo mode. We believe this was in part due to the low-count statistics of the nodal uptake as well as lack of probe shielding suggesting that the probe with its current design cannot be used for in-vivo lymph node localization and imaging.

In this manuscript, we reported the results generated by the first generation of the IBP platform where we successfully developed an intraoperative imaging probe which can provide high sensitivity to weak $\beta$ signal. This performance is mainly due to the use of high light yield scintillator and in-probe photodetector that eliminates potential light loss inherent to those designs using distant photodetectors (e.g. CCD or PMT) through optical fibers. Our detector development approach is cost-effective in that the preparation time of the detector and pixelation is a matter of hours.

We believe that our probe is most helpful in small, targeted areas, along with its use to determine the adequacy of margin resection. These areas might include, but are not limited to, the skull base, carotid sheath, mediastinum, and/or those in close proximity to nerve trunks. In such areas, adequacy of excision may or may not require resection or sacrifice of critical structures, which can dramatically alter the surgical procedure and its outcome. One of the most exciting concepts in this form of intraoperative imaging is the potential to localize suspected areas of neoplastic disease that are currently detected by PET and are invisible to conventional imaging and the naked eye.

## ACKNOWLEDGMENT

The authors would like to thank Dr. Haris Kudrolli for fruitful conversations, Sara Freed for her input in housing design, Dr. Arkadiusz Sitek for proofreading the manuscript, as well as Yihong Kaufmann and Terri Alpe for their help in animal handling.

## REFERENCES

[1] S. Gioux, H. S. Choi, and J. V. Frangioni, "Image-guided surgery using invisible near-infrared light: Fundamentals of clinical translation," *Mol. Imaging*, vol. 9, no. 5, pp. 237–255, 2010.

[2] M. Ammirati, N. Vick, and Y. Liao *et al.*, "Effect of the extent of surgical resection on survival and quality of life in patients with supratorial glioblastomas and anaplastic astrocytomas," *Neurosurgery*, vol. 21, pp. 201–206, 1987.

[3] F. Daghighian, E. J. Hoffman, P. Shenderov, B. Eshaghian, S. Sieegl, and M. C. Phelps, "Interaoperative beta probe: A device for detecting tissues labeled with positron or beta emitting isotopes during surgery," *Med. Phys.*, vol. 21, pp. 153–157, 1994.

[4] R. R. Raylman and R. L. Wahl, "A fiber-optically coupled positron-sensitive surgical probe," *J. Nucl. Med.*, vol. 35, pp. 909–913, 1994.

[5] R. R. Raylman, "A solid-state intraoperative beta probe system," *IEEE Trans. Nucl. Sci.*, vol. 47, no. 4, pp. 1696–1703, Aug. 2000.

[6] H. B. Barber, H. H. Barrett, J. M. Woolfenden, K. J. Myers, and T. S. Hickernell, "Comparison of in vivo scintillation probes and gamma cameras for detection of small, deep tumors," *Phys. Med. Biol.*, vol. 34, pp. 727–739, 1989.

[7] J. M. Woolfendon and H. B. Barber, "Radiation detector probes for tumor localization using tumorseeking radioactive tracers," *Ame. J. Roentgenol.*, vol. 159, pp. 35–39, 1989.

[8] L. R. MacDonald, M. P. Tornai, C. S. Levin, J. Park, M. Atac, D. B. Cline, and E. J. Hoffman, "Investigation of the physical aspects of beta imaging probes using scintillating fibers and visible light," *IEEE Trans. Nucl. Sci.*, vol. 42, no. 4, pp. 1351–1357, Aug. 1995.

[9] M. P. Tornai, C. S. Levin, L. R. Macdonald, C. H. Holdsworth, and E. J. Hoffman, "A miniature phoswich detector for gamma-ray localization and beta imaging," *IEEE Trans. Nucl. Sci.*, vol. 45, no. 3, pp. 1166–1173, Jun. 1998.

[10] C. S. Levin, M. P. Tornai, L. R. MacDonald, and E. J. Hoffman, "Annihilation gamma-ray background characterization and rejection for a small beta ray camera imaging positron emitters," *IEEE Trans. Nucl. Sci.*, vol. 44, no. 3, pp. 1120–1126, Jun. 1997.

[11] E. J. Hoffman, M. P. Tornai, C. S. Levin, L. R. MacDonald, and C. H. Holdsworth, "A dual detector beta-ray imaging probe with gamma-ray background suppression for use in intra-operative detection of radiolabeled tumors," *Nucl. Instrum. Methods Phys. Res. A*, vol. 409, pp. 511–516, 1998.

[12] C. S. Levin, L. R. MacDonald, M. P. Tornai, E. J. Hoffman, and J. Park, "Optimizing light collection from thin scintillators used in a beta-ray camera for surgical use," *IEEE Trans. Nucl. Sci.*, vol. 43, no. 3, pp. 2053–2060, Jun. 1996.

[13] M. P. Tornai, L. R. MacDonald, C. S. Levin, S. Siegel, and E. J. Hoffman, "Design considerations and initial performance of a 1.2 $cm^2$ beta imaging intra-operative probe," *IEEE Trans Nucl Sci.*, vol. 43, no. 4, pp. 2326–2335, Aug. 1996.

[14] S. Yamamoto, "An intra-operative positron probe with background rejection capability for FDG-guided surgery," *Ann. Nucl. Med.*, vol. 19, pp. 23–28, 2005.

[15] F. Wawroschek, H. Vogt, D. Weckermann, T. Wagner, and R. Harzmann, "The sentinel node concept in prostate cancer–first results of gamma probe-guided sentinel lymph node localization," *Eur. Urol.*, vol. 36, pp. 595–600, 1998.

[16] F. Liu, R. Wiener, J. R. Saffer, G. M. Mayers, W. Kononenko, F. M. Newcomer, R. Van Berg, and J. S. Karp, "Performance evaluation of a 64-pixel positron-sensitive surgical probe in sentinel lymph node surgical environment," in *Proc. IEEE Nuclear Science Symp. Conf. Rec.*, 2004, vol. 6, pp. 3559–3564.

[17] S. Yamamoto, C. Seki, K. Kashikura, H. Fujita, T. Matsuda, R. Ban, and I. Kanno *et al.*, "Development of a high resolution beta camera for a direct measurement of positron distribution on brain surface," *IEEE Trans. Nucl. Sci.*, vol. 44, no. 4, pp. 1538–42, Aug. 1997.

[18] S. Pitre, L. Menard, M. Ricard, M. Solal, J. R. Carbay, and Y. Charon, "A hand-held imaging probe for radio-guided surgery: Physical performance and preliminary clinical experience," *Eur. J. Nucl. Med. Mol. Imaging*, vol. 30, pp. 339–343, 2003.

[19] P. Olcott, F. Habte, A. M. Foudray, and C. S. Levin, "Performance characterization of a miniature, high sensitivity gamma ray camera," *IEEE Trans. Nucl. Sci.*, vol. 54, no. 5, pp. 1492–1497, Oct. 2007.

[20] F. Scopinaro, A. Tofani, G. di Santo, B. Di Pietro, A. Lombardi, M. Lo Russo, A. Soluri, R. Massari, C. Trotta, and C. Amanti, "High-resolution, hand-held camera for sentinel-node detection," *Cancer Biotherapy Radiopharm.* , vol. 23, no. 1, pp. 43–52, Feb. 2008.

[21] S. C. Thacker, B. C. Stack, V. Lowe, V. Gaysinskiy, S. Cool, V. V. Nagarkar, and G. Entine, "A novel imaging beta probe for radio-guided surgery," in *Proc. IEEE Conf. Rec. Nucl. Sci. Symp. and Med. Imag. Conf.*, 2008, pp. 3875–3878.

[22] B. Singh, B. C. Stack, S. Thacker, V. Gaysinskiy, S. Cool, G. Entine, and V. V. Nagarkar, "In vivo imaging of lingual cancer in a rabbit model using a hand-held imaging beta probe," in *Proc. IEEE Conf. Rec. Nucl. Sci. Symp. and Med. Imag. Conf.*, 2009, pp. 3038–3041.

[23] H. Sabet, H. B. Bhandari, H. Kudrolli, S. R. Miller, and V. V. Nagarkar, "A method for fabricating high spatial resolution scintillator arrays," *IEEE Trans. Nucl. Sci.*, vol. 60, no. 2, pp. 1000–1005, Apr. 2013.

[24] C. S. Levin and E. J. Hoffman, "Calculation of positron range and its effect on the fundamental limit of positron emission tomography system spatial resolution," *Phys. Med. Biol.*, vol. 44, p. 781, 1999.

[25] CASINO simulation package [Online]. Available: http://www.gel.usherbrooke.ca/casino/What.html

[26] M. P. Tornai, C. N. Archer, A. G. Weisenberger, R. Wojcik, V. Popov, and S. Majewski *et al.*, "Investigation of microcolumnar scintillators on an optical fiber coupled compact imaging system," *IEEE Trans. Nucl. Sci.*, vol. 48, no. 3, pp. 637–644, Jun. 2001.

[27] V. V. Nagarkar, S. V. Tipnis, K. Shah, I. Shestakova, and S. Cherry, "A high efficiency pixelated detector for small animal PET," *IEEE Trans. Nucl. Sci.*, vol. 51, no. 3, pp. 801–804, Jun. 2004.

[28] H. Sabet, H. Kudrolli, B. Singh, and V. V. Nagarkar, "Laser pixelation of thick scintillation detectors for medical imaging applications," *Proc. SPIE*, vol. 8853, 2013, X-Ray Studies, Medical Applications of Radiation Detectors, 88530B.

[29] B. C. Stack, J. Ye, T. B. Bartel, G. Shafirstein, and C. Chen *et al.*, "Orthotopic VX rabbit tongue cancer model with FDG-PET and histologic characterization," *Head Neck*, vol. 35, no. 8, pp. 1119–23, 2013.